cyclobutanol, where cleavage of the strained four-membered ring is favored, and pivaldehyde, where elimination of CO from the pivaloyl radical is preferred.

The rate constants for all the alcohol and aldehyde reactions studied here are very similar, and the reactivity trends are inconsistent with the formation of alkyl radicals. The rate of oxidation of R_2CHOH to R_2CO depends slightly on the steric bulk of R, which suggests that prior coordination of the alcohol to CrO^{2+} may be required before hydride transfer occurs.

Acknowledgment. This work was supported by a grant from the National Science Foundation (CHE-9007283). Some of the results were obtained with the use of the facilities of the Ames Laboratory. S.L.S. acknowledges the Natural Sciences and Engineering Research Council of Canada for a 1967 Science and Engineering Scholarship. We are grateful to F. H. Westheimer for comments.

Registry No. CrO^{+2}, 136301-85-4; CH_3OH, 67-56-1; D_2, 7782-39-0; CH_3CH_2OH, 64-17-5; $(CH_3)_2CHOH$, 67-63-0; $CH_2{=}CHCH_2OH$, 107-18-6; $CH_3(CH_2)_2CH_2OH$, 71-36-3; $CH_3CH_2CH(OH)CH_3$, 78-92-2; $C_6H_5CH_2OH$, 100-51-6; $C_6H_5CH(OH)CH_3$, 98-85-1; $(C_6H_5)_2CHOH$, 91-01-0; $(4\text{-}CH_3O)C_6H_4CH_2OH$, 105-13-5; $(4\text{-}CH_3)C_6H_4CH_2OH$, 589-18-4; $(4\text{-}CF_3)C_6H_4CH_2OH$, 349-95-1; $(CH_3)_3CCH_2OH$, 75-84-3; HCO_2H, 64-18-6; $H_2C_2O_4$, 144-62-7; $(CH_3CH_2)_2O$, 60-29-7; CrO_2^{+2}, 34021-34-6; Cr^{+2}, 22541-79-3; O_2, 7782-44-7; $CrOOCr^{+4}$, 136301-86-5; $TlOH^{+2}$, 15823-78-6; $HCrO_4^-$, 15596-54-0; cyclobutanol, 2919-23-5; cyclopentanol, 96-41-3; formaldehyde hydrate, 53280-36-7; pivaldehyde, 630-19-3.

Chemistry of an (η^6-Metallabenzene)metal Complex, [(η^6-Ir=CH=C(Me)=CH=C(Me)=CH)(PEt_3)$_3$]Mo(CO)$_3$[1]

John R. Bleeke,* Laura A. Bass, Yun-Feng Xie, and Michael Y. Chiang

Contribution from the Department of Chemistry, Washington University, St. Louis, Missouri 63130. *Received September 20, 1991*

Abstract: "Iridabenzene", (Ir=CH=C(Me)=CH=C(Me)=CH)(PEt_3)$_3$ (**1**), displaces *p*-xylene from (η^6-*p*-xylene)Mo(CO)$_3$ in tetrahydrofuran solvent, producing (η^6-iridabenzene)Mo(CO)$_3$ (**2**). The solid state structure of **2** has been determined by a single-crystal X-ray diffraction study (monoclinic, $P2_1/n$, a = 9.897 (1) Å, b = 16.213 (3) Å, c = 20.937 (3) Å, β = 96.68 (1)°, V = 3336.7 (9) Å^3, Z = 4, R = 0.036, R_w = 0.042). The iridium center in **2** retains the square-pyramidal coordination geometry of parent compound **1**, but the Mo(CO)$_3$ moiety now occupies the formerly "open face" of the pyramid. In solution, the iridabenzene ring rotates with respect to the Mo(CO)$_3$ fragment. The barrier for this process ($\Delta G^\ddagger$) is estimated to be less than 8 kcal/mol. Treatment of **2** with PMe_3 or CO (L) results in clean replacement of one basal PEt_3 ligand and production of [(η^6-Ir=CH=C(Me)=CH=C(Me)=CH)(PEt_3)$_2$(L)]Mo(CO)$_3$ (**3**, L = PMe_3; **4**, L = CO). The solid state structure of **3** (monoclinic, $P2_1/n$, a = 10.005 (2) Å, b = 18.012 (3) Å, c = 17.055 (4) Å, β = 93.33 (2)°, V = 3068.3 (11) Å^3, Z = 4, R = 0.031, R_w = 0.041) confirms the basal coordination position of the PMe_3 ligand. As in **2**, solution-phase arene ring rotation in **3** and **4** is facile. Treatment of **2**–**4** with $HBF_4{\cdot}OEt_2$ leads to protonation of the metal centers and production of the novel μ-H heterobimetallic complexes, {[(η^6-Ir=CH=C(Me)=CH=C(Me)=CH)(PEt_3)$_2$(L)(μ-H)]Mo(CO)$_3$}$^+BF_4^-$ (**5**, L = PEt_3; **6**, L = PMe_3; **7**, L = CO). In the solid state structure of **6**·tetrahydrofuran (orthorhombic, $P2_12_12_1$, a = 10.200 (4) Å, b = 16.467 (9) Å, c = 22.023 (7) Å, V = 3699 (3) Å^3, Z = 4, R = 0.022, R_w = 0.029), the hydride ligand resides approximately trans to the axial phosphine on iridium but bends in slightly toward molybdenum, generating a P_{ax}–Ir–H angle of 173 (2)°. The Ir–H and Mo–H bond lengths are 1.77 (6) and 1.97 (7) Å, respectively. While solution-phase arene ring rotation still occurs in **5**–**7**, the barrier for this process ($\Delta G^\ddagger$) increases to ~13.5–15 kcal/mol.

Introduction

Several years ago we reported the high-yield synthesis of a stable metallabenzene complex, (Ir=CH=C(Me)=CH=C(Me)=CH)(PEt_3)$_3$ (**1**).[1b,2] The structural and spectroscopic features of this species clearly indicated the presence of an aromatic ring system. Fenske–Hall calculations showed that the π-bonding in this ring involved the participation of an iridium-based d orbital with the set of five carbon-based p orbitals.[3] Recently, we have begun to explore the reaction chemistry of iridabenzene **1** and have discovered that it can be readily coordinated to a Mo(CO)$_3$ moiety, producing [(η^6-Ir=CH=C(Me)=CH=C(Me)=CH)(PEt_3)$_3$]Mo(CO)$_3$ (**2**).[1e] In this paper, we describe the structure, spectroscopy, and reactivity of (metallabenzene)metal complex **2** and compare its chemistry to that of the parent complex **1**. Since **1** and **2** represents the first *matched pair* of metallabenzene and (metallabenzene)metal complexes,[4] they afford a unique opportunity for comparative study.

Scheme I

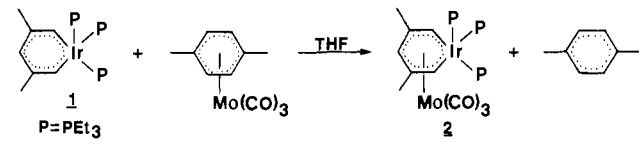

(1) Metallacyclohexadiene and Metallabenzene Chemistry. 6. For previous papers in this series: see: (a) Bleeke, J. R.; Peng, W.-J. *Organometallics* **1987**, *6*, 1576. (b) Bleeke, J. R.; Xie, Y.-F.; Peng, W.-J.; Chiang, M. *J. Am. Chem. Soc.* **1989**, *111*, 4118. (c) Bleeke, J. R.; Peng, W.-J.; Xie, Y.-F.; Chiang, M. Y. *Organometallics* **1990**, *9*, 1113. (d) Bleeke, J. R.; Haile, T.; Chiang, M. Y. *Organometallics* **1991**, *10*, 19. (e) Bleeke, J. R.; Xie, Y.-F.; Bass, L.; Chiang, M. Y. *J. Am. Chem. Soc.* **1991**, *113*, 4703. See, also: Bleeke, J. R. *Acc. Chem. Res.* **1991**, *24*, 271.

(2) Metallabenzenes are very rare. Only one other stable metallabenzene complex has been reported. See: Elliott, G. P.; Roper, W. R.; Waters, J. M. *J. Chem. Soc., Chem. Commun.* **1982**, 811,

(3) Bleeke, J. R.; Clayton, T. W., Jr., to be published.

(4) One other example of (metallabenzene)metal complex has been reported. However, in this system the free metallabenzene was not available for comparative studies. See: Kralik, M. S.; Rheingold, A. L.; Ernst, R. D. *Organometallics* **1987**, *6*, 2612.

0002-7863/92/1514-4213$03.00/0

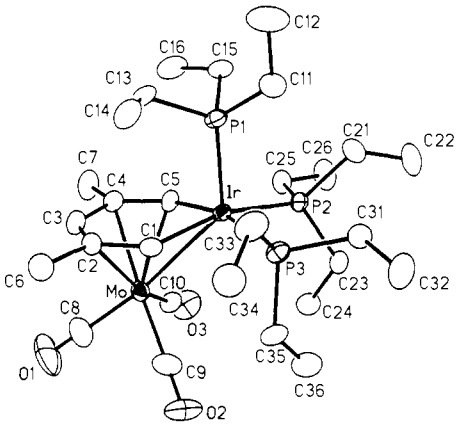

Figure 1. ORTEP drawing of $[(\eta^6\text{-Ir}{=}CH{-}C(Me){=}CH{-}C(Me){=}CH)(PEt_3)_3]Mo(CO)_3$ (**2**).

Results and Discussion

A. Synthesis and Structure of $[(\eta^6\text{-Ir}{=}CH{-}C(Me){=}CH{-}C(Me){=}CH)(PEt_3)_3]Mo(CO)_3$ (2). In 1979, Muetterties, Bleeke, and Sievert[5] reported that arene exchange in $(\eta^6\text{-arene})Mo(CO)_3$ complexes could be catalyzed by Lewis bases such as tetrahydrofuran and acetone. Typically, addition of arene′ and the Lewis base to a solution of $(\eta^6\text{-arene})Mo(CO)_3$ resulted in an equilibrium mixture of $(\eta^6\text{-arene})Mo(CO)_3$, $(\eta^6\text{-arene}')Mo(CO)_3$, and the free arenes. The position of the equilibrium depended on the basicity of the arenes involved; the most basic arenes gave rise to the most stable $(\eta^6\text{-arene})Mo(CO)_3$ complexes.

We now report that this arene exchange strategy can be used to synthesize $(\eta^6\text{-metallabenzene})Mo(CO)_3$ complexes in high yield. As shown in Scheme I, treatment of $(\eta^6\text{-}p\text{-xylene})Mo(CO)_3$ with iridabenzene **1** in tetrahydrofuran leads to clean replacement of the *p*-xylene ligand with arene **1** and production of $[(\eta^6\text{-Ir}{=}CH{-}C(Me){=}CH{-}C(Me){=}CH)(PEt_3)_3]Mo(CO)_3$ (**2**). None of the starting $(\eta^6\text{-}p\text{-xylene})Mo(CO)_3$ complex can be detected by NMR in the crude reaction mixture, indicating that the arene exchange equilibrium lies far to the right. This, in turn, suggests that arene **1** is far more basic than *p*-xylene.

The solid state structure of **2**, derived from a single-crystal X-ray diffraction study, is shown in Figure 1.[6] Significant bond distances and angles are given in Table I. The square-pyramidal coordination geometry of the parent iridabenzene **1**[1b] is still evident in the structure of compound **2**, although the $Mo(CO)_3$ moiety now occupies the formerly "open face" of the square pyramid. Furthermore, the four basal ligands (C1/C5/P2/P3) have been pushed up toward the iridium center, so that iridium lies only 0.29 Å above the basal plane in **2**, while it resides 0.41 Å above the same plane in **1**. As in **1**, the axial phosphine in **2** is bonded more tightly to iridium than are the basal phosphines (Ir–P1 = 2.274 (2) Å, while Ir–P2 = 2.365 (2) Å and Ir–P3 = 2.369 (2) Å).

The bonding within the metallabenzene ring in **2** is still fully delocalized, but the average C–C and Ir–C bond distances (1.41 and 2.03 Å, respectively) are slightly longer than those in parent **1** ($C{-}C_{av}$ = 1.38 Å, $Ir{-}C_{av}$ = 2.00 Å). The aromatic ring remains essentially planar, with the largest deviation from the least-squares plane being 0.10 Å.

The molybdenum atom is strongly π-complexed to all six atoms of the arene ring. The Mo–Ir distance is 2.978 (1) Å,[7] while the $Mo{-}C_{ring}$ distances range from 2.318 (10) to 2.404 (9) Å; the shortest bond is with C3. The three carbonyl groups, when projected onto the arene ring, approximately eclipse C1, C3, and C5.

Table I. Selected Bond Distances (Å) and Bond Angles (deg) with Estimated Standard Deviations for $[(\eta^6\text{-Ir}{=}CH{-}C(Me){=}CH{-}C(Me){=}CH)(PEt_3)_3]Mo(CO)_3$ (**2**)

Bond Distances

Ir–P1	2.274 (2)	C2–C3	1.411 (14)	Mo–C3	2.318 (10)
Ir–P2	2.365 (2)	C2–C6	1.521 (13)	Mo–C4	2.355 (9)
Ir–P3	2.369 (2)	C3–C4	1.429 (13)	Mo–C5	2.349 (9)
Ir–Mo	2.978 (1)	C4–C5	1.393 (12)	Mo–C8	1.932 (11)
Ir–C1	2.025 (8)	C4–C7	1.509 (14)	Mo–C9	1.961 (11)
Ir–C5	2.038 (9)	Mo–C1	2.397 (8)	Mo–C10	1.947 (10)
C1–C2	1.399 (13)	Mo–C2	2.404 (9)		

Bond Angles

P1–Ir–P2	96.6 (1)	Mo–Ir–C5	51.8 (2)
P1–Ir–P3	100.6 (1)	C1–Ir–C5	85.1 (4)
P1–Ir–Mo	132.9 (1)	Ir–C1–C2	132.2 (7)
P1–Ir–C1	101.3 (2)	C1–C2–C3	121.2 (8)
P1–Ir–C5	92.1 (3)	C2–C3–C4	125.8 (8)
P2–Ir–P3	95.4 (1)	C3–C4–C5	121.8 (8)
P2–Ir–Mo	110.9 (1)	C4–C5–Ir	131.0 (7)
P2–Ir–C1	161.7 (2)	Ir–Mo–C8	170.9 (4)
P2–Ir–C5	90.8 (3)	Ir–Mo–C9	101.2 (3)
P3–Ir–Mo	113.4 (1)	Ir–Mo–C10	104.4 (3)
P3–Ir–C1	84.8 (3)	C2–Mo–C10	160.0 (4)
P3–Ir–C5	165.2 (3)	C4–Mo–C9	170.3 (4)
Mo–Ir–C1	53.2 (2)		

B. Spectroscopy of $[(\eta^6\text{-Ir}{=}CH{-}C(Me){=}CH{-}C(Me){=}CH)(PEt_3)_3]Mo(CO)_3$ (2). In solution, iridabenzene complex **1** undergoes a very low-energy fluxional process, which exchanges the axial and basal phosphine ligands.[1b] Hence, even at −80 °C, the $^{31}P\{^1H\}$ NMR spectrum of **1** is a sharp singlet. Although the detailed mechanism of this process is not known, pseudorotation and turnstile processes can be envisaged.[8] Coordination of **1** to $Mo(CO)_3$ completely shuts down the intramolecular phosphine exchange process. Hence, the room temperature $^{31}P\{^1H\}$ NMR spectrum of **2** consists of a doublet (equivalent basal phosphines) and a triplet (axial phosphine), and no broadening of these signals is observed upon heating to 60 °C.

The ^1H NMR signals for the ring protons in **2** shift upfield from their positions in the parent metallabenzene **1**, as is normally observed when arenes coordinate to metal fragments. Protons H1/H5 in **2** appear at δ 8.08 (vs δ 10.91 in **1**), while H3 resonates at δ 6.25 (vs δ 7.18 in **1**). The ring carbon atoms show a similar upfield ^{13}C NMR shift. Hence, C1/C5, C2/C4, and C3 resonate at δ 135.7, 107.9, and 99.5 in **2** vs δ 167.3, 132.0, and 129.8 in **1**.

In compound **1**, the ^1H NMR signal for the α ring hydrogens (H1/H5) is a binomial quartet due to coupling to the three equivalent (rapidly exchanging) phosphine ligands.[1b] The observed coupling constant, 7.3 Hz, is an average of the three H–P coupling constants: $J_{H\text{-}P_{axial}}$, $J_{H\text{-}P_{cis/basal}}$, and $J_{H\text{-}P_{trans/basal}}$. Likewise, the $^{13}C\{^1H\}$ NMR resonance for C1/C5 in **1** is a binomial quartet with J = 30.2 Hz. In compound **2**, on the other hand, the intramolecular phosphine exchange process is completely stopped. The H1/H5 signal is a doublet (J = 20.7 Hz), due to strong coupling to a single phosphine, while C1/C5 is a doublet of doublets (J = 74.5, 9.4 Hz), due to strong coupling to one phosphine and weak coupling to a second phosphine. NMR experiments performed on $[(\eta^6\text{-Ir}{=}CH{-}C(Me){=}CH{-}C(Me){=}CH)(PEt_3)_2(CO)]Mo(CO)_3$ (**4**) (vide infra) have shown conclusively that the strong H–P coupling involves the cis/basal phosphine, while the strong C–P coupling involves the trans/basal phosphine.

In most $(\eta^6\text{-arene})Mo(CO)_3$ complexes, arene ring rotation occurs with only a small activation barrier.[9] Complex **2** is no

(5) Muetterties, E. L.; Bleeke, J. R.; Sievert, A. C. *J. Organomet. Chem.* **1979**, *178*, 197.

(6) A preliminary report of this structure has been communicated in ref 1e.

(7) Other recently reported Mo–Ir single bond distances range from 2.835 (2) to 2.902 (2) Å. However, most of these bonds are bridged by carbonyl or chloro ligands. See: (a) Churchill, M. R.; Li, Y.-J.; Shapley, J. R.; Foose, D. S.; Uchiyama, W. S. *J. Organomet. Chem.* **1986**, *312*, 121. (b) Mague, J. T.; Johnson, M. P. *Organometallics* **1990**, *9*, 1254.

(8) For a discussion of these processes as applied to the trigonal-bipyramidal case, see: Cotton, F. A.; Wilkinson, G. *Advanced Inorganic Chemistry*; 4th ed.; John Wiley and Sons: New York, 1980; pp 1218–1221.

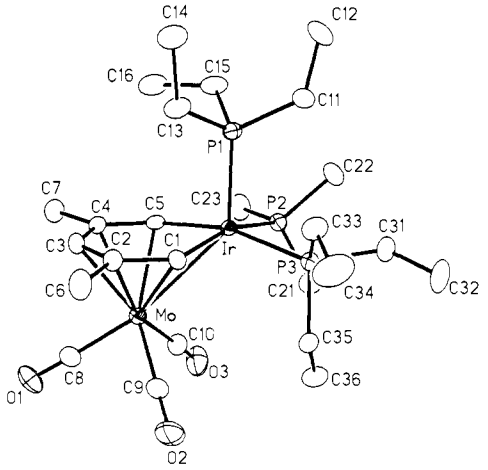

Figure 2. ORTEP drawing of $[(\eta^6\text{-}Ir{=}CH{-}C(Me){=}CH{-}C(Me){=}CH)(PEt_3)_2(PMe_3)]Mo(CO)_3$ (**3**).

Scheme II

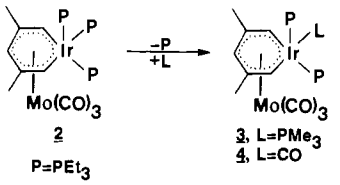

exception; the metallabenzene ring rotates freely with respect to the $Mo(CO)_3$ fragment. As a result, the carbonyl carbon atoms in **2** give rise to a single sharp peak in the $^{13}C\{^1H\}$ NMR spectrum, even at −80 °C. We calculate an upper limit of about 8 kcal/mol for the arene rotation process.[10]

The infrared spectrum of **2** shows the presence of two intense ν(CO) bands (A_1 and E), as is characteristic of (η^6-arene)Mo-$(CO)_3$ complexes.[11] The very low energy of these bands (1918 and 1836 cm^{-1}) indicates substantial π-backbonding and reflects the extremely electron-rich nature of arene **1**. By comparison, the ν(CO) bands for (η^6-*p*-xylene)$Mo(CO)_3$ appear at 1975 and 1901 cm^{-1}.[12]

C. Ligand Replacement Reactions. Synthesis and Structure of $[(\eta^6\text{-}Ir{=}CH{-}C(Me){=}CH{-}C(Me){=}CH)(PEt_3)_2(L)]Mo(CO)_3$ (3, L = PMe_3; 4, L = CO). Iridabenzene **1** undergoes facile ligand replacement reactions with PMe_3 and CO (L), producing species of formula $(Ir{=}CH{-}C(Me){=}CH{-}C(Me){=}CH)(PEt_3)_2(L)$. Only *one* PEt_3 ligand is replaced, even when excess PMe_3 or CO is employed.[13] In each case, the unique ligand L resides in a *basal* coordination site.[14] However, a low-energy fluxional process exchanges the two PEt_3 ligands, causing the molecules to *appear* to possess mirror-plane symmetry by NMR, even at low temperature.

Similarly, treatment of $[(\eta^6\text{-}Ir{=}CH{-}C(Me){=}CH{-}C(Me){=}CH)(PEt_3)_3]Mo(CO)_3$ (**2**) with PMe_3 or CO in refluxing tetrahydrofuran or acetone leads to clean replacement of one PEt_3 ligand and production of $[(\eta^6\text{-}Ir{=}CH{-}C(Me){=}CH{-}C(Me){=}CH)(PEt_3)_2(L)]Mo(CO)_3$ (**3**, L = PMe_3; **4**, L = CO) (see Scheme II). These species can also be produced via arene exchange by treating the performed ligand-substituted iridabenzenes, $(Ir{=}CH{-}C(Me){=}CH{-}C(Me){=}CH)(PEt_3)_2(L)$ (L = PMe_3 or CO), with (*p*-xylene)$Mo(CO)_3$ in tetrahydrofuran. As in the parent compounds, the unique ligand L in compounds **3** and **4** resides in a basal coordination site. This ligand arrangement is evident from the $^{31}P\{^1H\}$ NMR spectra which show separate resonances for the two PEt_3 ligands in each case. The structure of **3** has been confirmed by X-ray diffraction (see Figure 2 and Table II). Compound **3** is isostructural with **2**, and bond distances and angles within the two compounds are very similar (compare Tables I and II).

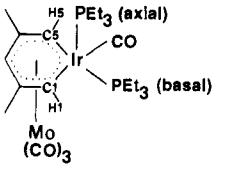

4

Figure 3. Drawing of $[(\eta^6\text{-}Ir{=}CH{-}C(Me){=}CH{-}C(Me){=}CH)(PEt_3)_2(CO)]Mo(CO)_3$ (**4**). C5 and H1 couple strongly to the basal PEt_3 ligand in the $^{13}C\{^1H\}$ and ^1H NMR spectra of **4**.

Scheme III

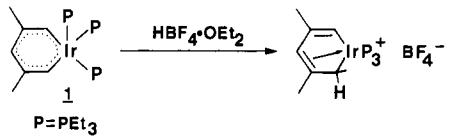

Scheme IV

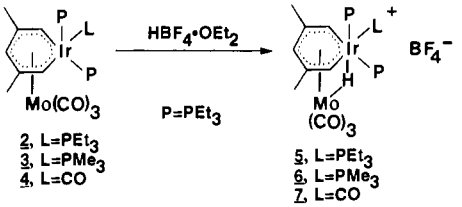

D. Spectroscopy of $[(\eta^6\text{-}Ir{=}CH{-}C(Me){=}CH{-}C(Me){=}CH)(PEt_3)_2(L)]Mo(CO)_3$ (3, L = PMe_3; 4, L = CO). While the general NMR spectral features of **3** and **4** are similar to those of **2**, described earlier, compound **4**'s spectra are particularly instructive because only one phosphine ligand (and therefore one ^{31}P nucleus) resides in the basal plane. This has enabled us to examine closely the individual ring H–P and ring C–P couplings. In compound **4** (see Figure 3), one of the α-ring carbons (C1) is trans to the basal CO and therefore does *not* exhibit strong C–P coupling. The other α ring carbon (C5) resides *trans* to the basal PEt_3 ligand and is strongly coupled ($J_{C\text{-}P}$ = 66.7 Hz).[15] Furthermore, one of the α hydrogens is strongly coupled to phosphorus while the other is not. Using ^{13}C–^1H heteronuclear-correlated (HETCOR) 2-D NMR techniques, we have shown that the strongly coupled proton signal correlates with C1 (the uncoupled carbon), while the uncoupled proton signal correlates with C5 (the strongly coupled carbon). Hence, H1 is strongly coupled ($J_{H\text{-}P}$ = 22.8 Hz) to the cis/basal phosphine, while H5 is uncoupled due to its cis orientation to the carbonyl. The origin of the strong coupling between α hydrogen and cis/basal phosphine is not completely clear but may result in part from the fact that the dihedral angle H_α–C_α–Ir–$P_{cis/basal}$ is approximately 0°. Large vicinal coupling constants are, of course, predicted by the Karplus equation[16] for nuclei with this orientation.

(9) Mann, B. E. In *Comprehensive Organometallic Chemistry*; Wilkinson, G.; Stone, F. G. A., Abel, E. W., Eds.; Pergamon: Oxford, 1982; Vol. 3, pp 89–113.

(10) In this calculation, we make the assumption that the chemical shift separation of the carbonyls in the stopped-exchange limit would be similar to that observed for the protonated analogue (vide infra).

(11) Davis, R.; Kane-Maguire, L. A. P. In *Comprehensive Organometallic Chemistry*; Wilkinson, G., Stone, F. G. A., Abel, E. W., Eds.; Pergamon: Oxford, 1982; Vol. 3, pp 1210–1220.

(12) Barbeau, C.; Turcotte, J. *Can. J. Chem.* **1976**, *54*, 1612.

(13) This strongly suggests that the ligand replacement reaction proceeds via a dissociative mechanism, i.e., loss of PEt_3 followed by addition of L.

(14) This ligand arrangement has been confirmed by X-ray crystallography in the case where L = $P(OMe)_3$: Bleeke, J. R.; Xie, Y.-F.; Chiang, M. Y., to be published.

(15) As expected, C1 resonates substantially downfield from C5 (δ 143.9 vs δ 125.1), since C1 resides trans to an electron-withdrawing CO group, while C5 resides trans to an electron-donating PEt_3 group.

Table II. Selected Bond Distances (Å) and Bond Angles (deg) with Estimated Standard Deviations for

$[(\eta^6\text{-Ir}{=}\text{CH}{=}\text{C(Me)}{=}\text{CH}{=}\text{C(Me)}{=}\text{CH})(PEt_3)_2(PMe_3)]Mo(CO)_3$ (**3**)

Bond Distances

Ir–P1	2.259 (2)	C2–C3	1.395 (10)	Mo–C3	2.336 (6)
Ir–P2	2.343 (2)	C2–C6	1.526 (10)	Mo–C4	2.384 (6)
Ir–P3	2.366 (2)	C3–C4	1.422 (9)	Mo–C5	2.380 (6)
Ir–Mo	2.950 (1)	C4–C5	1.409 (9)	Mo–C8	1.950 (8)
Ir–C1	2.031 (6)	C4–C7	1.502 (10)	Mo–C9	1.934 (8)
Ir–C5	2.027 (6)	Mo–C1	2.390 (6)	Mo–C10	1.950 (7)
C1–C2	1.409 (9)	Mo–C2	2.363 (7)		

Bond Angles

P1–Ir–P2	95.1 (1)	Mo–Ir–C5	53.3 (2)
P1–Ir–P3	100.1 (1)	C1–Ir–C5	85.7 (3)
P1–Ir–Mo	136.1 (1)	Ir–C1–C2	131.0 (5)
P1–Ir–C1	102.3 (2)	C1–C2–C3	122.9 (6)
P1–Ir–C5	93.6 (2)	C2–C3–C4	125.7 (6)
P2–Ir–P3	96.5 (1)	C3–C4–C5	121.6 (6)
P2–Ir–Mo	110.9 (1)	C4–C5–Ir	131.5 (5)
P2–Ir–C1	162.4 (2)	Ir–Mo–C8	163.4 (2)
P2–Ir–C5	90.4 (2)	Ir–Mo–C9	110.3 (2)
P3–Ir–Mo	110.8 (1)	Ir–Mo–C10	90.8 (2)
P3–Ir–C1	83.5 (2)	C2–Mo–C10	162.1 (3)
P3–Ir–C5	164.1 (2)	C4–Mo–C9	157.9 (3)
Mo–Ir–C1	53.6 (2)		

Arene ring rotation in **3** and **4** is facile. As with **2**, a single sharp peak is observed in the carbonyl region of the $^{13}C\{^1H\}$ NMR spectrum, even at −80 °C. Therefore, the rotational barrier, ΔG^*, is less than 8 kcal/mol.[10]

The infrared spectrum of **3** exhibits ν(CO) bands almost identical to those of **2** (1918 and 1835 cm^{-1}). On the other hand, the CO region of the IR spectrum of **4** looks quite different. First, there is a new band at 1977 cm^{-1} due to the carbonyl on iridium. Second, the A_1 and E bands due to the carbonyls on molybdenum are shifted to higher energy as a result of the decreased basicity of the arene. Finally, the E band is split into two peaks (1871 and 1846 cm^{-1}).

E. Protonation Reactions. Synthesis and Structure of $\{[(\eta^6\text{-Ir}{=}\text{CH}{=}\text{C(Me)}{=}\text{CH}{=}\text{C(Me)}{=}\text{CH})(PEt_3)_2(L)(\mu\text{-H})]Mo(CO)_3\}^+BF_4^-$ (5, L = PEt_3; 6, L = PMe_3; 7, L = CO). Treatment of iridabenzene **1** with the strong acid, $HBF_4{\cdot}OEt_2$, leads to protonation of the α ring carbon and production of $[(\text{Ir}{-}\text{CH}{=}\text{C(Me)}{-}\text{CH}{=}\text{C(Me)}{-}\text{CH}_2)(PEt_3)_3]^+BF_4^-$ (see Scheme III).[17] It is not known whether the proton attacks C_α directly or whether it attacks the iridium center and migrates to C_α. Attachment of $Mo(CO)_3$ to the arene ring in **1** blocks the addition of H^+ to the α ring carbon. Hence, treatment of $[(\eta^6\text{-Ir}{=}\text{CH}{=}\text{C(Me)}{=}\text{CH}{=}\text{C(Me)}{=}\text{CH})(PEt_3)_3]Mo(CO)_3$ (**2**) with $HBF_4{\cdot}OEt_2$ leads to protonation at the metal centers and production of the novel heterobimetallic μ-hydride complex $\{[(\eta^6\text{-Ir}{=}\text{CH}{=}\text{C(Me)}{=}\text{CH}{=}\text{C(Me)}{=}\text{CH})(PEt_3)_3(\mu\text{-H})]Mo(CO)_3\}^+BF_4^-$ (**5**) (see Scheme IV).[18] Similarly, treatment of **3** and **4** with $HBF_4{\cdot}OEt_2$ produces the μ-hydride complexes $\{[(\eta^6\text{-Ir}{=}\text{CH}{=}\text{C(Me)}{=}\text{CH}{=}\text{C(Me)}{=}\text{CH})(PEt_3)_2(L)(\mu\text{-H})]Mo(CO)_3\}^+BF_4^-$ (**6**, L = PMe_3; **7**, L = CO) (Scheme IV). The structure of compound **6** has been established through a low-temperature (−150 °C) X-ray diffraction study (see Figure 4). Significant bond distances and angles are given in Table III.

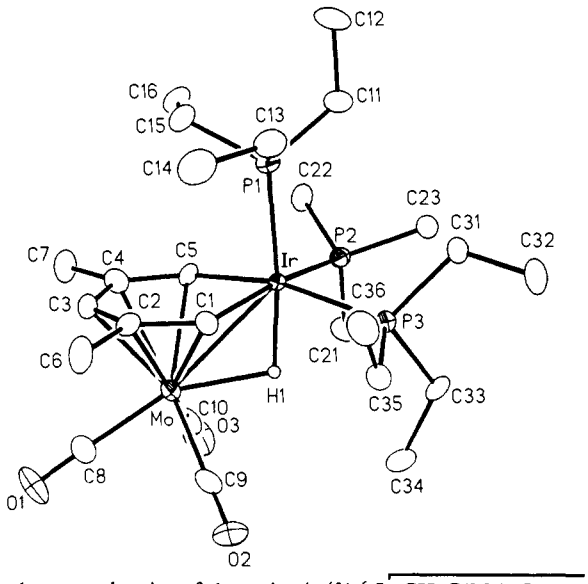

Figure 4. ORTEP drawing of the cation in $\{[(\eta^6\text{-Ir}{=}\text{CH}{=}\text{C(Me)}{=}\text{CH}{=}\text{C(Me)}{=}\text{CH})(PEt_3)_2(PMe_3)(\mu\text{-H})]Mo(CO)_3\}^+BF_4^-{\cdot}C_4H_8O$ (**6**).

Table III. Selected Bond Distances (Å) and Bond Angles (deg) with Estimated Standard Deviations for

$\{[(\eta^6\text{-Ir}{=}\text{CH}{=}\text{C(Me)}{=}\text{C(Me)}{=}\text{CH})(PEt_3)_2(PMe_3)(\mu\text{-H})]Mo(CO)_3\}^+ BF_4^-{\cdot}C_4H_8O$ (**6**)

Bond Distances

Ir–P1	2.323 (2)	C2–C3	1.429 (8)	Mo–C3	2.279 (6)
Ir–P2	2.360 (2)	C2–C6	1.499 (7)	Mo–C4	2.351 (6)
Ir–P3	2.360 (2)	C3–C4	1.410 (8)	Mo–C5	2.334 (5)
Ir–H1	1.771 (64)	C4–C5	1.384 (7)	Mo–C8	1.968 (6)
Ir–Mo	2.854 (2)	C4–C7	1.520 (8)	Mo–C9	2.011 (6)
Ir–C1	2.058 (5)	Mo–H1	1.972 (67)	Mo–C10	1.997 (6)
Ir–C5	2.053 (5)	Mo–C1	2.329 (5)		
C1–C2	1.383 (7)	Mo–C2	2.367 (5)		

Bond Angles

Ir–H1–Mo	99.2 (30)	H1–Ir–C5	82.6 (21)
P1–Ir–P2	98.6 (1)	Mo–Ir–C1	53.7 (1)
P1–Ir–P3	98.8 (1)	Mo–Ir–C5	53.9 (1)
P1–Ir–H1	173.0 (22)	C1–Ir–C5	85.6 (2)
P1–Ir–Mo	130.7 (1)	Ir–C1–C2	131.4 (4)
P1–Ir–C1	91.4 (1)	C1–C2–C3	120.9 (5)
P1–Ir–C5	95.1 (1)	C2–C3–C4	127.6 (5)
P2–Ir–P3	92.5 (1)	C3–C4–C5	121.5 (5)
P2–Ir–H1	87.9 (21)	C4–C5–Ir	131.5 (4)
P2–Ir–Mo	114.5 (1)	Ir–Mo–C8	168.2 (2)
P2–Ir–C1	168.1 (1)	Ir–Mo–C9	104.2 (2)
P2–Ir–C5	87.2 (2)	Ir–Mo–C10	105.2 (2)
P3–Ir–H1	83.5 (21)	H1–Mo–C8	154.0 (18)
P3–Ir–Mo	114.3 (1)	H1–Mo–C9	79.8 (19)
P3–Ir–C1	92.2 (1)	H1–Mo–C10	80.2 (18)
P3–Ir–C5	166.0 (1)	C2–Mo–C10	165.0 (2)
H1–Ir–Mo	43.0 (21)	C4–Mo–C9	162.8 (2)
H1–Ir–C1	81.8 (21)		

The basic structural features of **6** are very similar to those of its neutral parent, **3**. The iridabenzene ring remains coordinated to molybdenum in an η^6-fashion. The molybdenum–iridium bond in **6** shortens to 2.854 (2) Å (from 2.950 (1) Å in **3**). Likewise, the Mo–C_{ring} bonds in **6** shorten slightly, averaging 2.33 Å as compared to 2.37 Å in **3**. The hydride ligand, which was located in electron-difference maps and refined, bridges between Ir and Mo. The Ir–H and Mo–H bond lengths are 1.77 (6) and 1.97 (7) Å, respectively, while the Ir–H–Mo angle is 99 (3)°. The hydride resides approximately trans to the axial phosphine on iridium (P1) but bends in slightly toward molybdenum generating a P1–Ir–H angle to 173 (2)°. The influence of the trans hydride ligand causes the Ir–P1 bond in **6** to lengthen to 2.323 (2) from 2.259 (2) Å in **3**.

(16) (a) Karplus, M. *J. Chem. Phys.* **1959**, *30*, 11. (b) Karplus, M. *J. Am. Chem. Soc.* **1963**, *85*, 2870.

(17) The analogous trifluoromethanesulfonate salt has been reported in ref 1a.

(18) Treatment of (arene)$M(CO)_{3-x}(PR_3)_x$ (arene = benzene, toluene, mesitylene, etc.; M = Cr, Mo, W; x = 0, 1) complexes with strong acid leads, in general, to protonation at the metal center. See, for example: (a) Davison, A.; McFarlane, W.; Pratt, L.; Wilkinson, G. *J. Chem. Soc.* **1962**, 3653. (b) Fedorov, L. A.; Petrovskii, P. V.; Fedin, E. I.; Barenetskaya, N. K.; Zdanovich, V. I.; Setkina, V. N.; Kursanov, D. N. *J. Organomet. Chem.* **1975**, *99*, 297. (c) Flood, T. C.; Rosenberg, E.; Sarhangi, A. *J. Am. Chem. Soc.* **1977**, *99*, 4334.

Table IV. X-ray Diffraction Structure Summary

	Crystal Parameters and Data Collection Summary		
compd	2	3	6
formula	$C_{28}H_{54}IrMoO_3P_3$	$C_{25}H_{48}IrMoO_3P_3$	$C_{25}H_{49}BF_4IrMoO_3P_3 \cdot C_4H_8O$
formula wt	819.8	777.7	937.6
crystal system	monoclinic	monoclinic	orthorhombic
space group	$P2_1/n$	$P2_1/n$	$P2_12_12_1$
a, Å	9.897 (1)	10.005 (2)	10.200 (4)
b, Å	16.213 (3)	18.012 (3)	16.467 (9)
c, Å	20.937 (3)	17.055 (4)	22.023 (7)
α, deg	90.0	90.0	90.0
β, deg	96.68 (1)	93.33 (2)	90.0
γ, deg	90.0	90.0	90.0
V, Å^3	3336.7 (9)	3068.3 (11)	3699 (3)
Z	4	4	4
crystal dimensions, mm	0.10 × 0.20 × 0.70	0.20 × 0.60 × 0.70	0.20 × 0.24 × 0.58
crystal color	orange-red	red	red
density$_{calcd}$, g/cm^3	1.632	1.683	1.684
radiation, Å	Mo Kα, 0.71073	Mo Kα, 0.71073	Mo Kα, 0.71073
scan type	ω	θ:2θ	ω
scan rate, deg/min in ω	variable; 4.88–9.77	variable; 3.50–14.65	variable; 2.93–14.65
scan range (ω)	1.20°	1.20° plus Kα separation	1.20°
2θ range, deg	3.5–55.0	3.0–50.0	3.5–50.0
data collected	h −12 → 12 k 0 → 21 l 0 → 27	h −11 → 11 k 0 → 21 l 0 → 20	h −10 → 0 0 → 12 k −15 → 0 and 0 → 19 l −20 → 0 0 → 26
total decay	none detected	none detected	none detected
temp	295 K	295 K	123 K
	Treatment of Intensity Data and Refinement Summary		
no. of data collected	8194	5502	5059
no. of unique data	7705	5132	4834
no. of data with $I > 3^*\ \sigma(I)$	4226	4023	4832
Mo Kα linear abs. coeff, cm^{-1}	45.03	48.93	40.89
abs. correction applied	semiempirical	semiempirical	semiempirical
data to parameter ratio	12.6:1	13.4:1	12.6:1
R^a	0.036	0.031	0.022
$R_w{}^a$	0.042[b]	0.041[c]	0.029[d]
GOF[e]	0.94	1.21	0.79

[a] $R = \sum||F_o| - |F_c||/\sum|F_o|$. $R_w = [\sum w(|F_o| - |F_c|)^2/\sum w|F_o|^2]^{1/2}$. [b] $w = [\sigma^2(F_o) + 0.0008(F_o)^2]^{-1}$. [c] $w = [\sigma^2(F_o) + 0.0007(F_o)^2]^{-1}$. [d] $w = [\sigma^2(F_o) + 0.0010(F_o)^2]^{-1}$. [e] GOF = $[\sum w(|F_o| - |F_c|)^2/(N_{observations} - N_{variables})]^{1/2}$.

F. Spectroscopy of $\{[(\eta^6\text{-}Ir{=}CH{-}C(Me){=}CH{-}C(Me){=}CH)(PEt_3)_2(L)(\mu\text{-}H)]Mo(CO)_3\}^+BF_4^-$ (5, L = PEt_3; 6, L = Me_3; 7, L = CO). The NMR spectra of **5–7** bear a close resemblance to those of their neutral parents, **2–4**. The major difference, of course, is the presence of an upfield resonance in the ^{1}H NMR spectra of **5–7** due to the hydride. In **5** and **6**, this resonance comes at δ −13.30 and δ −13.15, respectively, and in each case is a doublet ($J \approx 42$ Hz) of triplets ($J \approx 11$ Hz). The doublet coupling is due to the trans/axial phosphine (P1), and its relatively small magnitude (for a trans coupling) is probably a consequence of the μ-bridging character of the hydride. In **7**, the hydride resonance comes at δ −12.91 and is a doublet of doublets with $J_{H-trans-P}$ = 45.8 Hz and $J_{H-cis-P}$ = 10.0 Hz.

As is the case for compounds **2–4**, arene ring rotation in **5–7** occurs rapidly at room temperature. Hence, the molybdenum-bound carbonyls give rise to single (but broad) peaks in the room temperature $^{13}C\{^1H\}$ NMR spectra of **5–7**. However, unlike the neutral compounds, arene rotation in **5–7** can be arrested by cooling to −30 °C. Shown in Figure 5 is the carbonyl region of the $^{13}C\{^1H\}$ NMR spectrum of **5**, recorded over a temperature range of −30 °C to 50 °C. At −30 °C, the stopped-exchange limiting spectrum is observed: two sharp CO resonances in a 1:2 ratio. As the temperature is raised, these signals gradually broaden and coalesce, ultimately appearing as a sharp singlet in the 50 °C spectrum. Line shape simulations of these variable-temperature (VT) $^{13}C\{^1H\}$ NMR spectra have established a free energy of activation (ΔG^*) of 13.7 (4) kcal/mol for the arene rotation process in **5**.

Stopped-exchange limiting spectra can also be obtained by cooling compounds **6** and **7** to −30 °C. In each case, three sharp carbonyl resonances are observed in the −30 °C $^{13}C\{^1H\}$ NMR spectrum, due to the three inequivalent molybdenum-bound CO ligands. Upon warming, these signals broaden and coalesce. Free energies of activation for arene rotation in **6** and **7** are calculated to lie between 13.5 and 15 kcal/mol on the basis of VT-NMR line shape simulations.

The infrared ν(CO) bands in **5–7** are displaced to higher energy (as compared to **2–4**) due to reduced π-backbonding. For example, the ν(CO) bands in **5** appear at 2009, 1937, and 1913 cm^{-1}, while those in **2** come at 1918 and 1836 cm^{-1}.

Summary

In tetrahydrofuran solvent, the iridabenzene complex $(Ir{=}CH{-}C(Me){=}CH{-}C(Me){=}CH)(PEt_3)_3$ (**1**) displaces *p*-xylene from $(\eta^6\text{-}p\text{-xylene})Mo(CO)_3$, producing $[(\eta^6\text{-}Ir{=}CH{-}C(Me){=}CH{-}C(Me){=}CH)(PEt_3)_3]Mo(CO)_3$ (**2**). Compounds **1** and **2** represent the first matched pair of metallabenzene and (metallabenzene)metal complexes and provide a unique opportunity for comparing the physical and chemical properties of these two compound classes.

A comparison of the chemical shifts of the ring hydrogens and carbons in **1** and **2** shows substantial upfield shifting upon attachment of the $Mo(CO)_3$ moiety to the arene ring. Furthermore, while **1** undergoes facile intramolecular phosphine exchange, this process is completely arrested in compound **2**.

Compound **2**, like **1**, reacts with a variety of 2e$^-$ ligands L, including PMe_3 and CO, to produce the ligand-substituted complexes $[(\eta^6\text{-}Ir{=}CH{-}C(Me){=}CH{-}C(Me){=}CH)(PEt_3)_2(L)]Mo(CO)_3$ (**3**, L = PMe_3; **4**, L = CO). In each case, ligand L resides in a basal coordination site. While treatment of **1** with acid leads to protonation at an α ring carbon, protonation of **2–4** with $HBF_4 \cdot OEt_2$ occurs at the metal centers, producing the novel heterobimetallic μ-hydride complexes $\{[(\eta^6\text{-}Ir{=}CH{-}C(Me){=}CH{-}C(Me){=}CH)(PEt_3)_2(L)(\mu\text{-}H)]Mo(CO)_3\}^+BF_4^-$ (**5**, L = PEt_3; **6**, L = PMe_3; **7**, L = CO). In solution, compounds **2–7**

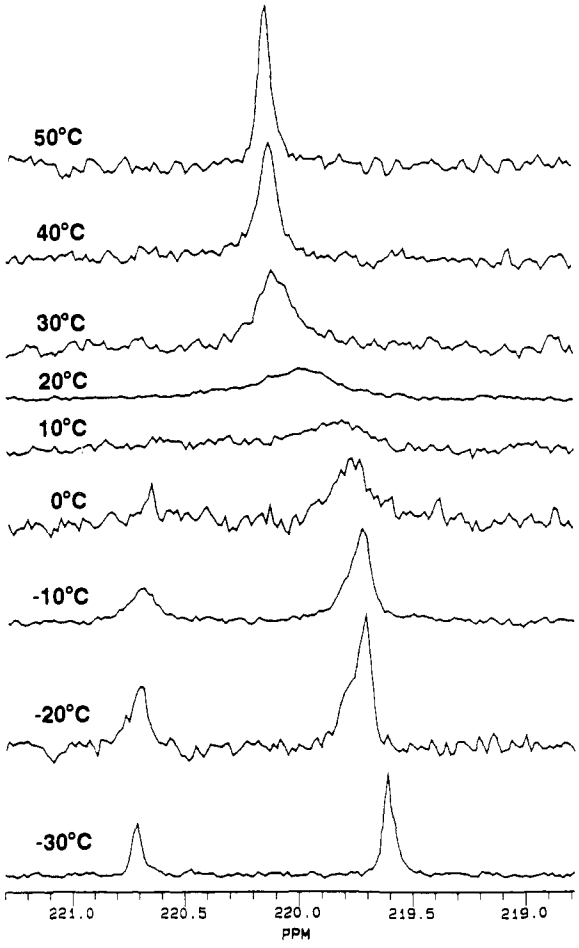

Figure 5. Carbonyl region of the $^{13}C\{^1H\}$ NMR spectrum of $\{[(\eta^6\text{-}Ir\overline{CH{=}C(Me){=}CH{=}C(Me){=}CH})(PEt_3)_3(\mu\text{-}H)]Mo(CO)_3\}^+BF_4^-$ (**5**), recorded over the temperature range of −30 °C to 50 °C. Line shape simulations of these variable-temperature spectra have established a free energy of activation ($\Delta G^\ddagger$) of 13.7 (4) kcal/mol for arene ligand rotation in **5**.

undergo arene rotation with respect to the $Mo(CO)_3$ moiety. The barrier ($\Delta G^\ddagger$) for rotation in the neutral complexes (**2–4**) is less than 8 kcal/mol, while that for the protonated complexes (**5–7**) is ~13.5–15 kcal/mol.

Experimental Section

General Comments. All manipulations were carried out under an inert atmosphere, with use of either drybox or Schlenk techniques. Diethyl ether and tetrahydrofuran were dried over sodium/benzophenone and distilled before use. Pentane was dried over calcium hydride and distilled. Acetone was dried over magnesium sulfate and distilled. Carbon monoxide (Air Products), trimethylphosphine (Strem), and tetrafluoroboric acid–diethyl ether (Aldrich) were used without further purification. $(Ir\overline{CH{=}C(Me){=}CH{=}C(Me){=}CH})(PEt_3)_3$ (**1**) was prepared as described earlier.[1b] (η^6-*p*-xylene)$Mo(CO)_3$[19] was synthesized by refluxing $Mo(CO)_6$ in *p*-xylene for 30 h and crystallized from methylene chloride.

All NMR experiments, except for those involving selective ^{31}P decoupling, were performed on a Varian XL-300 (^1H, 300 MHz; ^{13}C, 75 MHz; ^{31}P, 121 MHz) NMR spectrometer. Selective ^{31}P decoupling was done on a Varian VXR-500 NMR spectrometer. ^1H and ^{13}C spectra were referenced to tetramethylsilane. ^{31}P spectra were referenced to external H_3PO_4. Some of the ^1H peak assignments were made on the basis of selective ^{31}P decoupling experiments. Off-resonance decoupled ^{13}C spectra and ^{13}C–^1H shift-correlated (HETCOR) 2D spectra aided in assigning some of the ^1H and ^{13}C peaks.

Infrared spectra were recorded on a Mattson Polaris FT-IR spectrophotometer. Microanalyses were performed by Galbraith Laboratories, Inc., Knoxville, TN.

Dynamic NMR Studies. Determination of $\Delta G^\ddagger$. The $\Delta G^\ddagger$ values for iridabenzene rotation in compounds **5–7** were determined by NMR line shape simulation. The variable temperature $^{13}C\{^1H\}$ NMR spectra (CO region) were matched against theoretical line shapes, calculated using the method of C. S. Johnson.[20,21] In this way, exchange rate constants were determined for each temperatue. These exchange rate constants, K, were then used to calculate the free energy of activation, $\Delta G^\ddagger$, at each temperature, T, by using the Eyring equation.[22] The reported $\Delta G^\ddagger$ is the average value over all the temperatures in the simulation and the uncertainty is the estimated standard deviation.

Synthesis of $[(\eta^6\text{-}Ir\overline{CH{=}C(Me){=}CH{=}C(Me){=}CH})(PEt_3)_3]Mo(CO)_3$ (2). $(Ir\overline{CH{=}C(Me){=}CH{=}C(Me){=}CH})(PEt_3)_3$ (**1**) (0.25 g, 0.39 mmol) and (η^6-*p*-xylene)$Mo(CO)_3$ (0.11 g, 0.39 mmol) were dissolved in 30 mL of tetrahydrofuran and stirred at room temperature for 3 h. After removal of the solvent in vacuo, the reddish-orange residue was dissolved in a minimal quantity of acetone and cooled to −30 °C, causing **2** to crystallize as reddish-orange needles: yield 0.28 g, 87%; ^1H NMR (C_4D_8O, 17 °C) δ 8.08 (br d, $J_{H\text{-}P}$ = 20.7 Hz, 2, H1/H5), 6.25 (s, 1, H3), 2.07 (s, 6, ring CH_3's), 2.22–1.98 (m, 12, PEt_3 CH_2's), 1.80–1.62 (m, 6, PEt_3 CH_2's), 1.35–1.18 (m, 18, PEt_3 CH_3's), 0.95–0.82 (m, 9, PEt_3 CH_3's); $^{13}C\{^1H\}$ NMR (C_4D_8O, 17 °C) δ 229.8 (s, CO's), 135.7 (dd, $J_{C\text{-}P}$ = 74.5 Hz, 9.4 Hz, C1/C5), 107.9 (s, C2/C4), 99.5 (s, C3), 29.3 (s, ring CH_3's), 24.8–24.3 (m, PEt_3 CH_2's), 22.0–21.6 (m, PEt_3 CH_2's), 10.4, 9.0 (s's, PEt_3 CH_3's); $^{31}P\{^1H\}$ NMR (C_4D_8O, 17 °C) δ 18.8 (t, $J_{P\text{-}P}$ = 3.5 Hz, 1, axial PEt_3), −19.1 (d, $J_{P\text{-}P}$ = 3.5 Hz, 2, basal PEt_3's); IR (C_4H_8O, CO region) 1918, 1836 cm^{-1}. Anal. Calcd for $C_{28}H_{54}IrMoO_3P_3$: C, 41.02; H, 6.65. Found: C, 40.72; H, 6.70.

Synthesis of $(Ir\overline{CH{=}C(Me){=}CH{=}C(Me){=}CH})(PEt_3)_2(PMe_3)$. Trimethylphosphine (0.07 g, 0.94 mmol) was added to a stirred solution of compound **1** (0.60 g, 0.94 mmol) in acetone. After the solution was refluxed for 1 h, the solvent was removed in vacuo. The residue was then redissolved in a minimal quantity of acetone and cooled to −30 °C, causing $(Ir\overline{CH{=}C(Me){=}CH{=}C(Me){=}CH})(PEt_3)_2(PMe_3)$ to crystallize as red needles: yield 0.40 g, 71%; ^1H NMR ($CD_3C(O)CD_3$, 17 °C): δ 10.85 (d of t, $J_{H\text{-}PMe_3}$ = 15.0 Hz, $J_{H\text{-}PEt_3}$ = 5.0 Hz, 2, H1/H5), 7.14 (s, 1, H3), 2.50 (s, 6, ring CH_3's), 1.89–1.70 (m, 12, PEt_3 CH_2's), 1.66 (d, $J_{H\text{-}P}$ = 7.3 Hz, 9, PMe_3 CH_3's), 0.91–0.77 (m, 18, PEt_3 CH_3's); $^{13}C\{^1H\}$ NMR ($CD_3C(O)CD_3$, 17 °C): δ 167.9 (d of t, $J_{C\text{-}PMe_3}$ = 33.2 Hz, $J_{C\text{-}PEt_3}$ = 26.7 Hz, C1/C5), 132.5 (s, C2/C4), 129.7 (t, $J_{C\text{-}P}$ = 6.8 Hz, C3), 28.3 (s, ring CH_3's), 23.4–22.6 (m, PMe_3 CH_3's and PEt_3 CH_2's), 9.0 (s, PEt_3 CH_3's); $^{31}P\{^1H\}$ NMR ($CD_3C(O)CD_3$, 17 °C) δ 1.9 (d, $J_{P\text{-}P}$ = 10.3 Hz, 2, PEt_3's), −43.5 (t, $J_{P\text{-}P}$ = 10.3 Hz, 1, PMe_3). Anal. Calcd for $C_{22}H_{48}IrP_3$: C, 44.20; H, 8.11. Found: C, 42.74; H, 7.85.

Synthesis of $[(\eta^6\text{-}Ir\overline{CH{=}C(Me){=}CH{=}C(Me){=}CH})(PEt_3)_2(PMe_3)]Mo(CO)_3$ (3). Compound **2** (0.14 g, 0.17 mmol) was dissolved in 100 mL of acetone and PMe_3 (0.02 g, 0.26 mmol) was added. After the solution was refluxed for 3 h, the solvent was removed in vacuo. The residue was then dissolved in a minimal quantity of acetone and cooled to −30 °C, causing **3** to crystallize as reddish-orange needles: yield 0.11 g, 83%. (See Figure 2 for numbering scheme of ring C's and H's in the following spectra.) ^1H NMR (C_4D_8O, 17 °C) δ 8.35 (br d, $J_{H\text{-}PEt_3}$ = 21.7 Hz, 1, H1), 7.83 (br d, $J_{H\text{-}PMe_3}$ = 20.8 Hz, 1, H5), 6.32 (s, 1, H3), 2.09 (s, 6, ring CH_3's), 2.12–1.61 (m, 12, PEt_3 CH_2's), 1.74 (d, $J_{H\text{-}P}$ = 7.2 Hz, 9, PMe_3 CH_3's), 1.29–0.84 (m's, 18, PEt_3 CH_3's); $^{13}C\{^1H\}$ NMR (C_4D_8O, 17 °C) δ 230.2 (s, CO's), 140.1 (br d, $J_{C\text{-}PMe_3}$ = 73.2 Hz, C1), 132.5 (dd, $J_{C\text{-}PEt_3}$ = 71.7 Hz, $J_{C\text{-}P}$ = 7.2 Hz, C5), 108.4, 106.9 (s's, C2, C4), 99.9 (s, C3), 29.5 (d, $J_{C\text{-}P}$ = 6.5 Hz, ring CH_3), 29.1 (d, $J_{C\text{-}P}$ = 6.5 Hz, ring CH_3), 24.0 (d, $J_{C\text{-}P}$ = 28.3 Hz, PEt_3 CH_2's), 21.3 (d, $J_{C\text{-}P}$ = 24.2 Hz, PEt_3 CH_2's), 20.8 (d, $J_{C\text{-}P}$ = 27.3 Hz, PMe_3 CH_3's), 10.0, 8.7 (s's, PEt_3 CH_3's); $^{31}P\{^1H\}$ NMR (C_4D_8O, 17 °C) δ 18.4 (d, $J_{P\text{-}P}$ = 8.9 Hz, 1, axial PEt_3), −15.9 (d, $J_{P\text{-}P}$ = 15.0 Hz, 1, basal PEt_3), −49.4 (dd, $J_{P\text{-}P}$ = 15.0 Hz, 8.9 Hz, 1, PMe_3); IR (C_4H_8O, CO region) 1918, 1835 cm^{-1}. Anal. Calcd for $C_{25}H_{48}IrMoO_3P_3$: C, 38.60; H, 6.23. Found: C, 38.04; H, 6.19.

Synthesis of $(Ir\overline{CH{=}C(Me){=}CH{=}C(Me){=}CH})(PEt_3)_2(CO)$. A stream of carbon monoxide at 1 atm pressure was bubbled through a refluxing acetone solution of compound **1** (0.32 g, 0.50 mmol) for 1 h. Removal of the solvent under vacuum produced $(Ir\overline{CH{=}C(Me){=}CH{=}C(Me){=}CH})(PEt_3)_2(CO)$ as an orange-red oil: yield 0.19 g, 70%; ^1H NMR ($CD_3C(O)CD_3$, 17 °C) δ 11.26 (t, $J_{H\text{-}P}$ = 4.8 Hz, 2, H1/H5), 7.37 (br s, 1, H3), 2.50 (s, 6, ring CH_3's), 1.92–1.47 (m, 12, PEt_3 CH_2's),

(19) (a) Fischer, E. O.; Öfele, K.; Essler, H.; Fröhlich, W.; Mortensen, J. P.; Semmlinger, W. *Chem. Ber.* **1958**, *91*, 2763. (b) Strohmeier, W. *Chem. Ber.* **1961**, *94*, 3337.

(20) Johnson, C. S., Jr. *Am. J. Phys.* **1967**, *35*, 929.

(21) Martin, M. L.; Martin, G. J.; Delpuech, J.-J. *Practical NMR Spectroscopy*; Heydon: London, 1980; pp 303–309.

(22) Lowry, T. H.; Richardson, K. S. *Mechanism and Theory in Organic Chemistry*; Harper and Row: New York, 1976.

0.97–0.80 (m, 18, PEt_3 CH_3's); $^{13}C\{^1H\}$ NMR ($CD_3C(O)CD_3$, 17 °C) δ 171.7 (t, J_{C-P} = 23.5 Hz, C1/C5), 160.8 (s, CO), 135.3 (t, J_{C-P} = 8.0 Hz, C3), 134.8 (s, C2/C4), 27.1 (s, ring CH_3's), 22.4 (d, J_{C-P} = 30.3 Hz, PEt_3 CH_2's), 8.6 (s, PEt_3 CH_3's); $^{31}P\{^1H\}$ NMR ($CD_3C(O)CD_3$, 17 °C) δ 4.7 (s); IR (C_4H_8O, CO region) 1943 cm^{-1}.

Synthesis of $[(\eta^6\text{-}Ir\text{-}CH\text{-}C(Me)\text{-}CH\text{-}C(Me)\text{-}CH)(PEt_3)_2(CO)]Mo(CO)_3$ (4). Compound **2** (0.14 g, 0.17 mmol) was dissolved in 150 mL of tetrahydrofuran, and the resulting solution was refluxed for 6 h while carbon monoxide (1 atm) was bubbled vigorously through it. The solution was then cooled to room temperature and stirred overnight. After removal of the solvent, the residue was dissolved in diethyl ether and cooled to −30 °C, causing **4** to crystallize as reddish-orange needles: yield 0.10 g, 80%. (See Figure 3 for numbering scheme of ring C's and H's in following spectra.) ^1H NMR (C_4D_8O, 17 °C) δ 8.52 (br d, J_{H-P} = 22.8 Hz, 1, H1), 7.75 (s, 1 H5), 6.28 (s, 1, H3), 2.12 (s, 3, ring CH_3's), 2.05 (s, 3, ring CH_3's), 2.13–1.67 (m's, 12, PEt_3 CH_2's), 1.22–0.87 (m's, 18, PEt_3 CH_3's); $^{13}C\{^1H\}$ NMR (C_4D_8O, 17 °C) δ 228.0 (s, Mo CO's), 185.6 (d, J_{C-P} = 12.8 Hz, Ir CO), 143.9 (d, J_{C-P} = 8.3 Hz, C1), 125.1 (d, J_{C-P} = 66.7 Hz, C5), 110.4, 107.4 (s's, C2, C4), 99.3 (s, C3), 28.8 (m, ring CH_3's), 23.5 (d, J_{C-P} = 31.9 Hz, PEt_3 CH_2's), 20.5 (d, J_{C-P} = 27.3 Hz, PEt_3 CH_2's), 8.8, 8.0 (s's, PEt_3 CH_3's); $^{31}P\{^1H\}$ NMR (C_4D_8O, 17 °C) δ 16.7 (s, 1, axial PEt_3), −13.0 (s, 1, basal PEt_3); IR (C_4H_8O, CO region) 1977, 1929, 1871, 1846 cm^{-1}. Anal. Calcd for $C_{23}H_{39}IrMoO_4P_2$: C, 37.85: H, 5.40. Found: C, 36.94; H, 5.65.

Protonation of Compound 1. Synthesis of $[(Ir\text{-}CH{=}C(Me)\text{-}CH{=}C(Me)\text{-}CH_2)(PEt_3)_3]^+BF_4^-$. Cold (−30 °C) $HBF_4{\cdot}OEt_2$ (0.07 g, 0.44 mmol) was added dropwise to a cold (−78 °C) stirred solution of compound **1** (0.28 g, 0.44 mmol) in acetone. The color of the solution rapidly changed from red to light yellow. After removal of the solvent in vacuo, the residue was washed with cold diethyl ether and filtered, producing $[(Ir\text{-}CH{=}C(Me)\text{-}CH{=}C(Me)\text{-}CH_2)(PEt_3)_3]^+BF_4^-$ as a yellow powder: yield 0.22 g, 68%. The NMR spectra of this species were essentially identical to those of $[(Ir\text{-}CH{=}C(Me)\text{-}CH{=}C(Me)\text{-}CH_2)(PEt_3)_3]^+O_3SCF_3^-$, which was reported earlier (ref 1a).

Synthesis of $[(\eta^6\text{-}Ir\text{-}CH\text{-}C(Me)\text{-}CH\text{-}C(Me)\text{-}CH)(PEt_3)_3(\mu\text{-}H)]Mo(CO)_3]^+BF_4^-$ (5). Excess $HBF_4{\cdot}OEt_2$ (0.07 g, 0.42 mmol) was added to a cold (−30 °C) solution of compound **2** (0.13 g, 0.16 mmol) in tetrahydrofuran. After stirring briefly, the solution was stored at −30 °C for 16 h, causing **5** to precipitate. This precipitate was redisolved in acetone/diethyl ether and cooled to −30 °C, producing reddish needles of **5**; yield 0.09 g, 63%; ^1H NMR (CD_3CN, 19 °C) δ 7.89 (br d, J_{H-P} = 14.6 Hz, 2, H1/H5), 7.01 (s, 1, H3), 2.20 (s, 6, ring CH_3's), 2.28–2.12 (m, 12, PEt_3 CH_2's), 2.10–1.95 (m, 6, PEt_3 CH_2's), 1.35–1.26 (m, 18, PEt_3 CH_3's), 1.13–1.02 (m, 9, PEt_3 CH_3's), −13.30 (d of t, J_{H-P} = 42.1 Hz, 11.3 Hz, 1, hydride); $^{13}C\{^1H\}$ NMR (CD_3CN, 19 °C) δ 220.0 (br s, CO's), 132.9 (br d, J_{C-P} = 70.7 Hz, C1/C5), 114.5 (s, C2/C4), 98.4 (s, C3), 28.3 (s, ring CH_3's), 22.5 (d, J_{C-P} = 34.3 Hz, PEt_3 CH_2's), 19.2 (d, J_{C-P} = 30.3 Hz, PEt_3 CH_2's), 9.5 (s, PEt_3 CH_3's), 9.3 (s, PEt_3 CH_3's); $^{13}C\{^1H\}$ NMR (CD_3CN, −30 °C, CO region) δ 220.7 (s, CO under C3), 219.6 (s, CO's under C1/C5); $^{31}P\{^1H\}$ NMR (CD_3CN, 19 °C) δ −2.4 (t, J_{P-P} = 16.4 Hz, 1, axial PEt_3), −24.2 (d, J_{P-P} = 16.4 Hz, 2, basal PEt_3's); IR (CH_3CN, CO region) 2009, 1937, 1913 cm^{-1}. Anal. Calc'd for $C_{28}H_{55}BF_4IrMoO_3P_3$: C, 37.05; H, 6.12. Found: C, 37.24; H, 6.08.

Synthesis of $[(\eta^6\text{-}Ir\text{-}CH\text{-}C(Me)\text{-}CH\text{-}C(Me)\text{-}CH)(PEt_3)_2(PMe_3)(\mu\text{-}H)]Mo(CO)_3]BF_4^-$ (6). A procedure analogous to that described above for the synthesis of **5** was employed. Treatment of **3** (0.15 g, 0.19 mmol) with excess $HBF_4{\cdot}OEt_2$ (0.07 g, 0.42 mmol) produced **6**, which crystallized as red needles of **6**·THF from tetrahydrofuran solvent: yield 0.12 g, 69%. (Note: The THF solvate was removed by evacuation prior to obtaining the elemental analysis and recording the spectra. See Figure 4 for numbering scheme of ring C's and H's in the following spectra.) ^1H NMR (CD_3CN, 19 °C) δ 7.98 (d, J_{H-PMe_3} = 18.0 Hz, 1, H5), 7.92 (d, J_{H-PEt_3} = 15.0 Hz, 1, H1), 7.06 (s, 1, H3), 2.23 (s, 3, ring CH_3's), 2.21 (s, 3, ring CH_3's), 2.28–2.00 (m, 6, PEt_3 CH_2's), 1.97–1.77 (m, 6, PEt_3 CH_2's), 1.80 (d, J_{H-P} = 8.4 Hz, 9, PMe_3 CH_3's), 1.38–1.25 (m, 9, PEt_3 CH_3's), 1.13–0.99 (m, 9, PEt_3 CH_3's), −13.15 (d of t, J_{H-P} = 42.0 Hz, 11.4 Hz, 1, hydride); $^{13}C\{^1H\}$ NMR (CD_3CN, 19 °C) δ 220.3 (br s, CO's), 134.0 (br d, J_{C-PMe_3} = 72.3 Hz, C1), 132.5 (br d, J_{C-PEt_3} = 71.0 Hz, C5), 114.7 (s, C2 and C4), 98.8 (s, C3), 28.3 (s, ring CH_3), 28.2 (s, ring CH_3), 21.9 (d, J_{C-P} = 34.0 Hz, PEt_3 CH_2's), 19.1 (d, J_{C-P} = 32.0 Hz, PMe_3 CH_3's or PEt_3 CH_2's), 18.9 (d, J_{C-P} = 28.6 Hz, PEt_3 CH_2's or PMe_3 CH_3's), 9.2, 8.7 (s's, PEt_3 CH_3's); $^{13}C\{^1H\}$ NMR (CD_3CN, −30 °C, CO region) δ 220.8 (s), 220.2 (s), 219.9 (s); $^{31}P\{^1H\}$ NMR (CD_3CN, 19 °C) δ 1.2 (dd, J_{P-P} = 18.4 Hz, 16.5 Hz, 1, axial PEt_3), −22.3 (dd, J_{P-P} = 16.5 Hz, 12.2 Hz, 1, basal PEt_3), −49.0 (dd, J_{P-P} = 18.4 Hz, 12.2 Hz, 1, PMe_3); IR (CH_3CN, CO region) 2010, 1937, 1913 cm^{-1}. Anal. Calcd for $C_{25}H_{49}BF_4IrMoO_3P_3$: C, 34.69; H, 5.72. Found: C, 34.04; H, 5.79.

Synthesis of $[(\eta^6\text{-}Ir\text{-}CH\text{-}C(Me)\text{-}CH\text{-}C(Me)\text{-}CH)(PEt_3)_2(CO)(\mu\text{-}H)]Mo(CO)_3]^+BF_4^-$ (7). A procedure analogous to that described above for the synthesis of **5** was employed. Treatment of **4** (0.13 g, 0.18 mmol) with excess $HBF_4{\cdot}OEt_2$ (0.09 g, 0.55 mmol) produced **7** as a purple oil. Repeated treatment with diethyl ether gradually converted the oil to a free-flowing purple-red microcrystalline powder. Yield: 0.09 g, 60%. A numbering scheme analogous to that shown in Figure 3 is used for the ring C's and H's in the following spectra: ^1H NMR (CD_3CN, 19 °C) δ 8.19 (s, 1, H5), 7.49 (d, J_{H-P} = 18.1 Hz, 1, H1), 6.97 (s, 1, H3), 2.20–1.82 (m, 12, PEt_3 CH_2's), 2.14 (s, 3, ring CH_3's), 2.13 (s, 3, ring CH_3's), 1.24–1.10 (m, 9, PEt_3 CH_3's), 1.04–0.90 (m, 9, PEt_3 CH_3's), −12.91 (dd, J_{H-P} = 45.8 Hz, 10.0 Hz, 1, hydride); $^{13}C\{^1H\}$ NMR (CD_3CN, 19 °C) δ 219.4 (v br s, Mo CO's), 173.1 (t, J_{C-P} = 6.8 Hz, Ir CO), 125.5 (t, J_{C-P} = 6.6 Hz, C1), 124.1 (d, J_{C-P} = 62.5 Hz, C5), 117.1, 114.0 (s's, C2, C4), 99.0 (s, C3), 27.9 (s, ring CH_3), 27.4 (d, J_{C-P} = 6.2 Hz, ring CH_3), 22.0 (d, J_{C-P} = 36.7 Hz, PEt_3 CH_2's), 18.9 (d, J_{C-P} = 30.6 Hz, PEt_3 CH_2's), 8.8 (d, J_{C-P} = 4.9 Hz, PEt_3 CH_3's), 8.2 (d, J_{C-P} = 4.9 Hz, PEt_3 CH_3's); $^{13}C\{^1H\}$ NMR (CD_3CN, −30 °C, CO region) δ 219.9 (s), 219.3 (s), 217.9 (s); $^{31}P\{^1H\}$ NMR (CD_3CN, 19 °C) δ 6.5 (d, J_{P-P} = 12.7 Hz, 1, axial PEt_3), −16.9 (d, J_{P-P} = 12.7 Hz, 1, basal PEt_3); IR (CH_3CN, CO region) 2046, 2021, 1956, 1931 cm^{-1}.

Single-Crystal X-ray Diffraction Studies. Suitable crystals of compounds **2**, **3**, and **6** were mounted on glass fibers, and X-ray diffraction data were collected on a Siemens R3m/V diffractometer using graphite-monochromated Mo Kα radiation. All data reduction and refinement were done using the Siemens SHELXTL PLUS program package on a MicroVAX II computer.[23] Crystal data and details of data collection and structure analysis are summarized in Table IV.

In each structure determination, the position of most of the non-hydrogen atoms were obtained using direct methods. The structures were completed by successive full-matrix least-squares refinements and difference Fourier map calculations. In **2** and **3**, all non-hydrogen atoms, except for phosphine methyl carbon C34 in **2** (which exhibited a 2-fold disorder), were refined anisotropically. C34 (55% occupancy) and C34′ (45% occupancy) were refined isotropically. Most of the hydrogen atoms were placed at idealized positions, riding upon their respective carbon atoms, and a common isotropic temperature factor was refined. The three metallabenzene hydrogens in **2** (H1A, H3A, H5A) were located on electron-difference maps and positionally refined.

Compound **6** crystallized with a molecule of tetrahydrofuran (THF) solvent. All non-hydrogen atoms in **6** were refined anisotropically, while those in the THF molecule were refined isotropically. Two of the THF carbon atoms, C43 and C44, exhibited minor positional disorders and were refined with the following site occupancies: C43, 82%; C43′, 18%; C44, 76%; C44′, 24%. The three metallabenzene hydrogens (H1A, H3A, H5A) and the bridging hydrogen (H1) were located on electron-difference maps and positionally refined. All other hydrogens in **6** (but not the THF hydrogens) were placed at idealized positions, riding upon their respective carbon atoms. A common isotropic temperature factor was refined.

Acknowledgment. We thank the National Science Foundation (Grants CHE-8520680 and CHE-9003159) and the donors of the Petroleum Research Fund, administered by the American Chemical Society, for support of this research. A loan of $IrCl_3{\cdot}3H_2O$ from Johnson-Matthey Aesar/Alfa is gratefully acknowledged. Washington University's X-ray Crystallography Facility was funded by the National Science Foundation's Chemical Instrumentation Program (Grant CHE-8811456). The High Resolution NMR Service Facility was funded in part by National Institutes of Health Biomedical Support Instrument Grant 1 S10 RR02004 and by a gift from Monsanto Company.

Supplementary Material Available: Structure determination summaries and listings of final atomic coordinates, thermal parameters, bond lengths, and bond angles for **2**, **3**, and **6**, and ORTEP drawings showing the positions of disordered atoms in **2** and **6** (28 pages); tables of observed and calculated structure factor amplitudes for **2**, **3**, and **6** (65 pages). Ordering information is given on any current masthead page.

(23) Atomic scattering factors were obtained from the following: *International Tables for X-ray Crystallography*, Kynoch Press: Birmingham, England, 1974; Vol. IV.